Journal of the Korean Physical Society, Vol. 67, No. 1, July 2015, pp. 142∼146

Feasibility Study of the Neutron Dose for Real-time Image-guided Proton Therapy: A Monte Carlo Study

Jin Sung Kim, Jung Suk Shin, Daehyun Kim, Eunhyuk Shin, Kwangzoo Chung, Sungkoo Cho, Sung Hwan Ahn, Sanggyu Ju, Yoonsun Chung, Sang Hoon Jung and Youngyih Han*

Department of Radiation Oncology, Samsung Medical Center, Sungkyunkwan University School of Medicine, Seoul 135-710, Korea

(Received 8 December 2014, in final form 23 February 2015)

Two full rotating gantries with different nozzles (multipurpose nozzle with MLC, scanning dedicated nozzle) for a conventional cyclotron system are installed and being commissioned for various proton treatment options at Samsung Medical Center in Korea. The purpose of this study is to use Monte Carlo simulation to investigate the neutron dose equivalent per therapeutic dose, H/D, for X-ray imaging equipment under various treatment conditions. At first, we investigated the H/D for various modifications of the beamline devices (scattering, scanning, multi-leaf collimator, aperture, compensator) at the isocenter and at 20, 40 and 60 cm distances from the isocenter, and we compared our results with those of other research groups. Next, we investigated the neutron dose at the X-ray equipment used for real-time imaging under various treatment conditions. Our investigation showed doses of 0.07 ∼ 0.19 mSv/Gy at the X-ray imaging equipment, depending on the treatment option and interestingly, the 50% neutron dose reduction was observed due to multi-leaf collimator during proton scanning treatment with the multipurpose nozzle. In future studies, we plan to measure the neutron dose experimentally and to validate the simulation data for X-ray imaging equipment for use as an additional neutron dose reduction method.

PACS numbers: 87.53.Pb, 87.53.Wz, 87.50.Gi
Keywords: Proton therapy, Monte-Carlo simulation, Neutron dose
DOI: 10.3938/jkps.67.142

I. INTRODUCTION

Proton radiation has totally different dosimetric characteristics from those of conventional radiation therapy [1]. X-ray radiation exhibits an exponentially decaying energy deposition in tissue with increasing depth beyond a build-up region whereas protons exhibit an increasing energy deposition with the penetration depth, with a maximum energy deposition, the Bragg peak near the end of the proton beam range [2]. The spread-out Bragg peak, which indicates the region of maximum energy deposition, can be positioned within the target to create a conformal high-dose region. Although advanced photon radiotherapy, such as intensity-modulated radiotherapy and tomotherapy, can produce the same level of dose conformity across a tumor, proton beams have the advantage of decreasing the low-dose volume in the surrounding normal tissue [3, 4]. However, Hall reported that the secondary neutron dose was a critical problem with scattered proton therapy and that the cancer risk was higher than it was for IMRT treatment [5]. After that report, every proton therapy center calculated or measured their secondary neutron dose at different positions before their 1st treatment [6–13].

Recently, proton therapy systems have been adapting advanced image guidance systems that are used and proven technology in X-ray therapy fields such as cone-beam computed tomography (CBCT) and real-time tracking during treatment. Two full rotating gantries with different nozzles (multipurpose nozzle with multi-leaf collimator (MLC), and a scanning dedicated nozzle) with conventional cyclotron system are installed and are being commissioning for various proton treatment options at Samsung Medical Center in Korea. Because the X-ray flat-panel system is not located in the proton beam nozzle, X-ray imaging during treatment to check the position of tumor or any fiducial marker is possible, as shown in Fig. 1. Image-guided proton therapy with real-time X-ray imaging during proton treatment is one of most advanced treatment options, but secondary neutron exposure for this imaging technique has not been studied at all. The purpose of this study is to investigate the neutron dose equivalent per therapeutic dose, H/D, to the X-ray imaging equipment under various treatment conditions by using Monte Carlo simulations.

*E-mail: Youngyih@skku.edu; Fax: 82-2-3410-2619

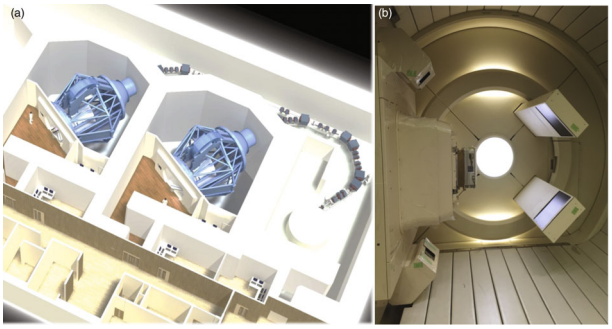

Fig. 1. (Color online) (a) Layout of the proton therapy center that has two conventional gantries with a cyclotron at Samsung Medical Center. (b) X-ray imaging system for the proton therapy machine, which has an option for real-time imaging during treatment.

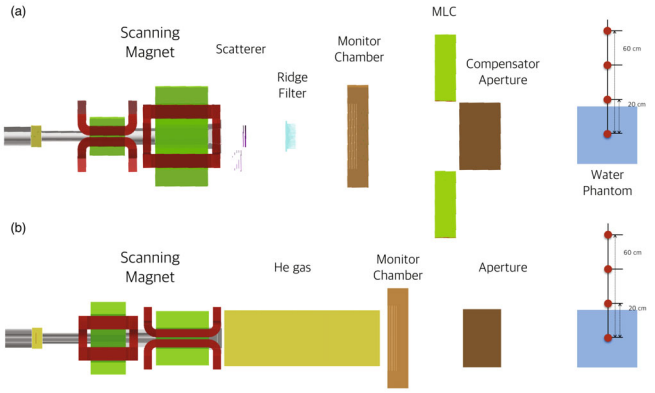

Fig. 2. (Color online) Schematic view of the two different proton beam delivery systems at Samsung Medical Center and the points at which the neutron dose per absorbed dose was calculated by using MCNP simulations: (a) multipurpose nozzle, which has both wobbling and scanning mode, and (b) pencil beam dedicated nozzle.

II. METHOD

We have two different nozzle structures to deliver the proton dose to a patients, a multipurpose nozzle and pencil beam scanning (PBS) dedicated nozzle, according to their lateral spreading method as shown in Fig. 2.

1. Wobbling Mode with the Multipurpose Nozzle

The two x- and y-wobbling magnets can generate a larger proton beam size by using circular movement at a fixed frequency, and the enlarged proton beam scatters to give a two-dimensional dose distribution, which is the actual field size. A proton beam with a pristine Bragg peak after the ridge filter can yield a spread-out Bragg peak (SOBP), and several combinations of ridge filters are needed because each ridge filter has only one SOBP value. The patient aperture and the multi-leaf collimator are a beam stoppers with a hole shaped to the outer projection of the target in the beam's eye view. The range compensator is a plastic block with material cut away in a complex shape. It is carefully aligned with the aperture and the patient's tumors, and tailors the dose in depth by shifting the proton range more or less depending on what part of the tumors, and the upstream tissues, a particular the proton beam is aimed at. Thus, we need all these combination of scatterer, ridge filter, MLC, compensator and aperture to deliver a wobbling beam to a patient.

2. Scanning Mode in Multipurpose Nozzle

When we use the scanning mode, we do not need all the equipment that is needed in the wobbling mode, such as the wobbling magnet, scatterer, ridge filter, MLC, compensator and aperture. We use only the scanning magnet for proton beam delivery. However, every component, especially the MLC unit, still exists in the nozzle and works as a neutron absorber if no collisions occur between protons and the components. Since recent advance in scanning proton treatment by using an aperture to reduce the penumbra were reported, this combination for the neutron dose distribution has been analyzed by using Monte Carlo simulations.

3. PBS dedicated Nozzle

The PBS dedicated nozzle is only used for scanning treatment and does not have any component to generate a neutron dose except a scanning magnet and a He gas duct. However, we also calculated the case in which a patient aperture is used to reduce the penumbra.

4. MCNP simulation

Monte Carlo studies with the MCMPX V2.5 code were performed based on the two different beam nozzle geometries (MLC, compensator, aperture, ridge filter, satterer, *etc.*) obtained from Sumitomo Heavy Industry, and a 40 $\times$ 30 $\times$ 30 cm^3 water phantom was simulated for 230 MeV proton beams and a 10-cm SOBP by using a 15 $\times$ 15 cm^2 brass aperture. At first, we investigated the value of the H/D for various modifications of the beam line devices (scatterer, scanning magnet, MLC, aperture, compensator) at the isocenter and at 20-, 40- and 60-cm distances from the isocenter, and we compared our results with those of other research groups. Next, we investigated the neutron dose at the X-ray equipment used for real-time imaging under various treatment conditions.

Table 1. Various treatment options (six options) with a combination of a MLC, compensator and block using two different nozzles at Samsung Medical Center.

Nozzle	Type	MLC	Compensator	Block	Treatment option
Multi-purpose Nozzle	Wobbling	O	O	X	MW1
		O	O	O	MW2
	Scanning	O	X	X	MS1
		O	X	O	MS2
PBS		X	X	X	PS1
Dedicated Nozzle		X	X	O	PS2

Table 2. Calculated neutron dose at different points for the various treatment options.

(mSv/Gy)	MW1	MW2	MS1	MS2	PS1	PS2
X-ray Tube	0.194	0.188	0.081	0.08	0.078	0.078
Detector	0.593	0.572	0.058	0.058	0.131	0.131
Isocenter	27.505	27.328	6.398	6.405	6.555	6.916
20 cm	3.463	3.13	0.392	0.351	0.492	0.417
40 cm	3.085	3.235	0.222	0.205	0.492	0.363
60 cm	1.788	1.764	0.168	0.173	0.404	0.363

The detailed information for each treatment condition is shown in Table 1. A schematic view of the two different proton beam delivery systems and the points whose neutron dose per absorbed dose were calculated by using MCNP simulations are shown in Fig. 2.

III. RESULTS AND DISCUSSION

1. Neutron Dose Distribution at the Isocenter Axis

Table 2 lists the neutron doses received at various distances from the isocenter that were obtained by using six different treatment options. Our simulations calculated the H/D values by using the scattering and the scanning methods at the isocenter and at 20, 40 and 60 cm from isocenter for six different treatment options and showed results comparable with these measured or simulated at other proton therapy centers, as shown in Fig. 3. We need to validate these Monte Carlo simulation results with actual neutron dose measurements; however, we can use our Monte Carlo simulation for relative dose comparisons to determine the effect of the neutron dose or to perform other systematic analyses.

Figure 4 shows the neutron dose per absorbed dose at the isocenter for all treatment options. Our simulation showed that the wobbling treatment mode (MW1, MW2) produced a relatively 429% higher neutron dose than the other scanning treatment mode (MS1, MS2, PS1, PS2) and that the results for neither the wobbling nor the scanning treatment mode had any significant dependency on the use of a block or a MLC.

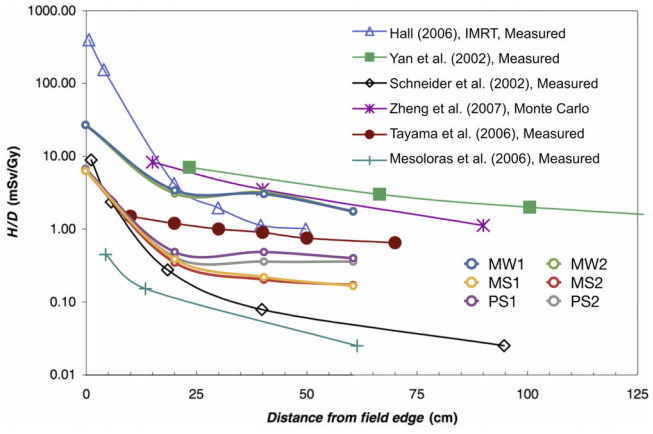

Fig. 3. (Color online) Comparison of the radiation dose equivalent per therapeutic dose as a function of the distance from the field edge. The six calculated options and other measured results are shown.

2. Neutron Dose at the X-Ray Imaging Equipment

Figure 5 shows the neutron dose per proton absorbed dose at the X-ray tube and at the flat-panel detector for

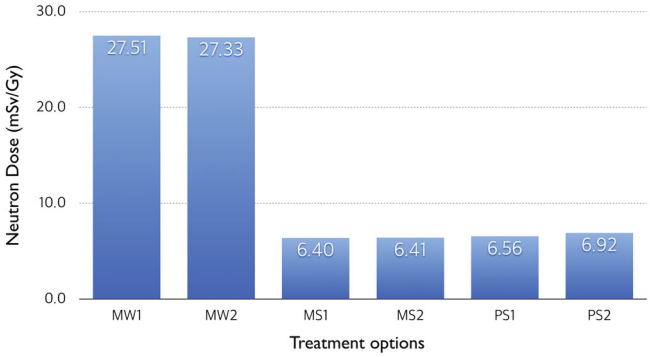

Fig. 4. (Color online) Simulated neutron dose equivalent per proton absorbed dose (mSv/Gy) at the isocenter for six different treatment options. The wobbling mode has a relatively higher neutron dose than the scanning mode.

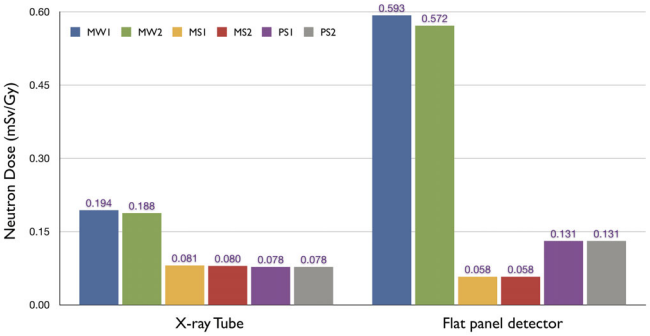

Fig. 5. (Color online) Simulated neutron dose equivalent per proton absorbed dose (mSv/Gy) at the X-ray imaging equipment including the X-ray tube and flat panel detector.

real-time image-guided proton therapy. Our investigation showed neutron doses of the 0.08 ∼ 0.19 mSv/Gy at the real-time X-ray tube and 0.06 ∼ 0.59 mSv/Gy at the flat-panel detector, depending on the treatment option, and the neutron doses were relatively higher for the wobbling treatment mode. Although no significant dependence on the use of the aperture was observed, a neutron dose reduction effect of more than 50% was interestingly observed at the flat-panel detector for the proton scanning treatment option with the multipurpose nozzle (MS1, MS2). Because the difference between MS1, MS2 and PS1, PS2 is the presence of the MLC, we think that the MLC behaves as a neutron absorber, especially in the scanning treatment mode with a multipurpose nozzle

3. Neutron Dose in the Nozzle Component and the Neutron Spectrum

The neutron dose contributions from each component in the nozzles are different. Thus, our calculated neutron doses at several different points in the two different nozzles types (profile monitor, scatterer, ridge filter, dose monitor, MLC, compensator, *etc.*) for the wobbling

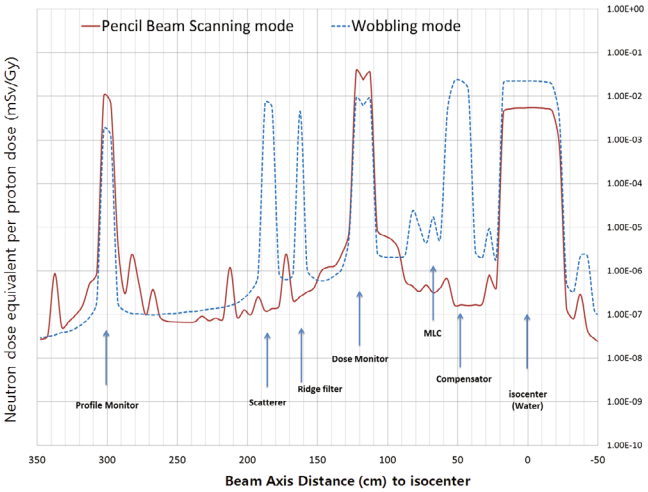

Fig. 6. (Color online) Calculated neutron dose for the two different nozzles at several different points in the nozzle for the wobbling and the pencil beam scanning modes.

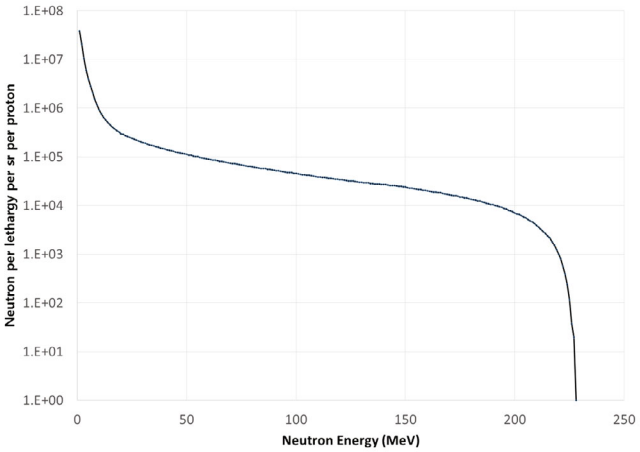

Fig. 7. (Color online) Neutron energy spectrum used in this study after MCNP parameterization for the neutron generated angle and energy.

mode and the pencil-beam scanning mode are shown in Fig. 6. The only main neutron sources in the scanning mode are the only two dose monitors in the beam nozzle. We used the MCNP parameterization for the neutron-generated angle and energy by using ptrac file information in order to reduce the Monte Carlo simulation time, and the resulting neutron spectrum is shown in Fig. 7.

IV. CONCLUSION

The neutron dose to the iso-center and to the X-ray equipment for real-time imaging under various proton treatment conditions were simulated for the first time at Samsung Medical Center. These are valuable reference data that can be directly compared with corresponding

data for proton therapy in the literature. In future studies, we plan to measure the neutron dose experimentally and to validate our simulation data for X-ray imaging equipment for use as an additional neutron dose reduction method for real-time image guided proton therapy.

ACKNOWLEDGMENTS

This research was supported by the Nuclear Safety Research Program through the Korea Radiation Safety Foundation (KORSAFe) and the Nuclear Safety and Security Commission (NSSC), Republic of Korea (Grant No. 1402015), by the National Research Foundation of Korea (NRF) funded by the Ministry of Science, ICT & Future Planning (2012M3A9B6055201 and 2012R1A1A2042414) and by a Samsung Medical Center grant [GFO 1130081].

REFERENCES

[1] J. S. Kim *et al.*, J. Korean Phys. Soc, **55**, 1640 (2009).
[2] J. S. Shin *et al.*, Radiation Oncology Journal **29**, 206 (2011).
[3] D. W. Miller, Medical physics **22**, 1943 (1995).
[4] D. R. Olsen *et al.*, Radiotherapy and Oncology **83**, 123 (2007).
[5] E. J. Hall, Int. J. Radiat. Oncol. Biol. Phys. **65**, 1 (2006).
[6] R. Macklis, Int. J. Radiat. Oncol. Biol. Phys. **66**, 1593 (2006).
[7] Y. Zheng *et al.*, Phys. Med. Biol. **52**, 4481 (2007).
[8] S. Yonai *et al.*, Medical physics **36**, 4830 (2009).
[9] X. Wang *et al.*, Int. J. Radiat. Oncol. Biol. Phys. **76**, 1563 (2010).
[10] M. Yoon *et al.*, Int. J. Radiat. Oncol. Biol. Phys. **77**, 1477 (2010).
[11] E. S. Diffenderfer *et al.*, Medical physics **38**, 6248 (2011).
[12] S. Kim *et al.*, Radiotherapy and oncology **98**, 335 (2011).
[13] Y. Zheng *et al.*, Medical physics **39**, 3484 (2012).